Bottom-up construction of *in vitro* switchable memories

Supplementary Information Appendix

Adrien Padirac[1], Teruo Fujii[1], Yannick Rondelez[1,*]

[1]LIMMS/CNRS-IIS, Institute of Industrial Science, The University of Tokyo, 4-6-1 Komaba, Meguro-ku, Tokyo 153-8505,

*Correspondence to: rondelez@iis.u-tokyo.ac.jp

Table of Contents

I. Workflow of network assembly with the DNA-toolbox

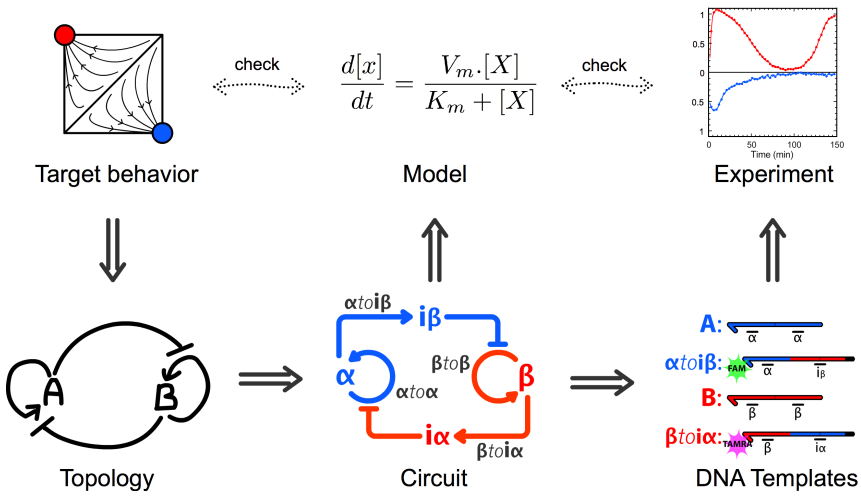

Figure S1: Implementation of a target behavior with the DNA-toolbox. A target behavior can correspond to one out of a number of network topologies. These topologies can in turn be translated into an assembly of modules compatible with the toolbox. A simple model of the corresponding circuit allows one to check the consistency of the chosen design with the target behavior, and find out the key parameters or conditions that the circuit must meet in order to perform as expected. The following step consists in the design of the templates that encode the activation, autocatalysis and inhibition modules of the circuit, and the experimental implementation. The experiment should be in good agreement with the simple (or more detailed) model, which can in turn be used to adjust the experimental parameters of the circuit.

II. Experimental building of the bistable circuit

1. Design rules

To build the bistable, we started with the autocatalytic template included in a recently reported oscillator (template β*to*β) (23). We then designed another sequence (α) with several constraints: the sequences must be orthogonal (this also goes for their respective inhibitors), in order to avoid reaction crosstalk. Also, sequences should not exhibit a nicking recognition site at an unwanted location. As suggested by the simple model, we designed inhibitors so that their dissociation constant was about two orders of magnitude higher than that of input strands (Table S3). Inhibitors are 15 bases long: 13 bases are matched with the target template, and the last two 3' bases are mismatched, preventing the polymerase from extending the duplex. Inhibitors should not display the nicking enzyme recognition site: to meet this requirement, 7 of the 13 matched bases are on the template input (3') side and 6 on its output (5') side: two partial but no complete recognition sites are then included in these strands (See Table S2).

Because of the symmetric topology of the bistable circuit, both autocatalytic modules should be of equivalent "strength". Thus, we designed α and β so that the predicted[1] melting temperatures (T_m) on their templates were as close as possible: even though the T_m alone is not enough to determine the relative "strength" of α and β, it is an accessible parameter to balance the sequences before assembling the circuit. Enzymes have a different affinity for each sequence, and this parameter is not predictable (but has recently attracted interest in the context of isothermal DNA amplification and template dependence (60)), nor controllable for a given sequence. A robust network design should then be as little sensitive as possible to such unpredictable parameters in delivering the target function, and also provide some adjustable control parameters that may be used to mitigate these effects, once the sequences have been decided. Here we have shown that it is possible – in a certain extent – to tune the concentrations of some templates to experimentally "balance" a non-perfect system in order to obtain a robust bistable circuit.

Monitoring of α and β is done by using N-quenching (47): a single fluorophore is attached at the 3' end of templates α*to*iβ and β*to*iα, where its fluorescence gets modified by the presence of the template's input (i.e. single-strand vs double-strand state). On the contrary, the binding of the output doesn't impact the fluorescence of the template 3' fluorophore (47). The fluorophores were not attached to templates α*to*α or β*to*β for the following reason: these two autocatalytic modules are the target of inhibitors iα and iβ, which hybridize 4 bases away from the template 3' fluorophore. In this configuration, they might induce a slight fluorescence change when hybridizing (47). To avoid this unwanted effect, we attached the fluorophores on inhibition modules α*to*iβ and β*to*iα.

[1] Using DINAMelt (http://mfold.rna.albany.edu/?q=DINAMelt)

2. Protection from ttRecJ

In order to protect template from degradation by 5'->3' exonuclease ttRecJ, templates have several phosphorothioate backbone modifications (PT) at their 5' end. Note that the RecJ exonuclease used here is not the same as the commercially available enzyme from *Escherichia coli* used in Montagne *et al*. (23). Here we used thermophilic analog ttRecJ from *T. thermophilus* (45, 46). This thermophilic enzyme is more stable than its mesophilic counter part. Therefore it does not require the addition of stabilizing additives in the buffer and extends the range of available working temperatures.

However the activities of the two enzymes are slightly different. Figure S2 shows the degradation of 400 nM of template β*to*β in presence of the same concentration of ttRecJ as used in the switch experiments reported here. Even with 2 PTs, β*to*β is rapidly degraded, which may prematurely disrupt the functioning of a circuit containing it (this stands in contrast with the mesophilic RecJ, for which two phophorothioates were found to provide a good protection (23)). Three terminal consecutive PTs appear to be necessary to obtain a correct protection, but produce a problematic side-effect: the nicking enzyme cutting speed is divided by roughly a factor of 4 in the presence of the third PT (Fig. S3-*B*).

We hypothesized that this was the consequence of a form of competitive inhibition, where the nicking enzyme could bind –unproductively– the recognition sequence on the output side of the template (even if for this pseudo-site, no DNA extends beyond the nicking position). Following this line of thought, we searched for a way to decrease the affinity of the nicking enzyme for the output site. We found that replacing the thymine of the recognition sequence by an uracil (GACUC instead of GACTC) could indeed address the reduced cutting speed issue. In this case, a correct nicking rate was recovered (Fig. S3-*C*). In fact, we even observed an increase in the rate of the nicking process, compared to template β*to*β with 2 PT and no dU.

Also, when a U was placed in the input (3') site of the template, the nicking enzyme was mostly unable to cut the duplex anymore (Fig. S3-*C*): this confirms that in these conditions, a modified recognition site is poorly processed by the nicking enzyme. Altogether, these observations strongly support the previous hypothesis about competitive inhibition. For a more complete analysis of the effect of dT->dU modifications on various endonuclease activities, see the work of Mazurek and Sowers (61).

Note that we are discussing about dT->dU modifications, and not the dynamic incorporation of dUTP instead of dTTP, as in other PCR-related strategies (62). The presence of these modifications on the templates will not affect the other toolbox-related processes because i) T->U has only a small effect on duplex stability, and ii) many DNA polymerases -except archaeal (63)- simply ignore the difference between dT and dU on the template and reliably incorporate a dATP at this position. We thus adopted this strategy: all activation and autocatalytic templates have three PTs at their 5'-end, and a U in their output recognition site.

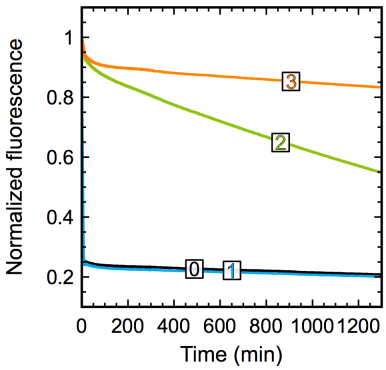

Figure S2: Degradation of template βtoβ (400 nM) by ttRecJ in the same buffer, ttRecJ concentration (50 nM) and temperature (42 °C) as for the bistable switch, memory and push-push memory experiments. Template βtoβ has 0, 1, 2 or 3 consecutive phosphorothioate backbone modifications at its 5' end.

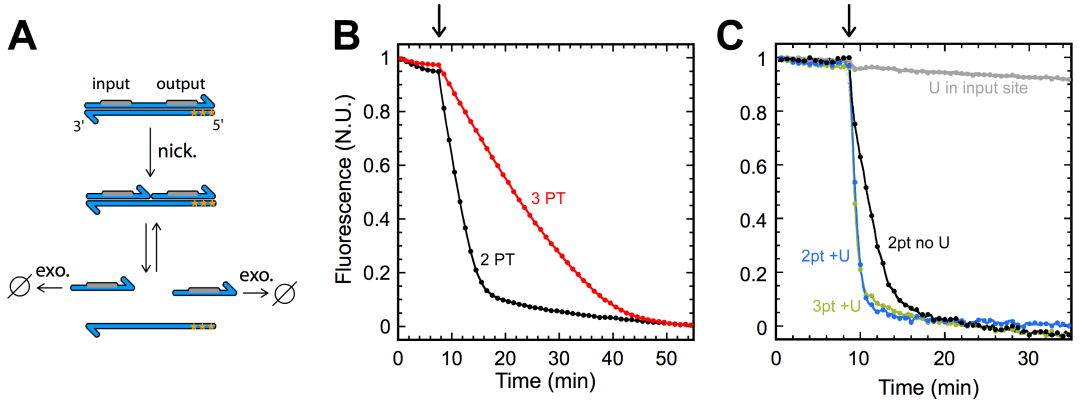

Figure S3: Assay for nicking enzyme activity measurement depending on various template modifications. (A) Assay schematic: in the presence of templates in duplex form, the nicking enzyme (nick.) cuts the upper strand between input and output. The two resulting short strands can dissociate from the template and are degraded by an exonuclease (exo.) to avoid the accumulation of products. In the presence of Evagreen (double-strand specific intercalating dye) this reaction results in a global decrease of fluorescence, as template duplexes are converted to single-stranded form. The nicking event is the rate-limiting step. Stars represent phosphorothioate backbone modifications (PT), located at the 5'-end of the template. (B) and (C): Normalized fluorescence records for various templates modifications. The arrow indicates the time for injection of nicking enzyme i.e. the start of the reaction. (B) The presence of 3 PTs slows down the reaction, even if they are very far from the actual nicking site. (C) With a U in the nicking enzyme output recognition site (i.e. the one that has no function), 2 PTs (blue) or 3 PTs (green) do not slow down the enzyme activity. U-containing templates are even faster than the template with 2 PT and unmodified output recognition site (black).

3. DNA sequences

DNA templates used in this study, and their concentrations, are shown in Table S1. Input and inhibitors (i.e. the species that are dynamically produced and degraded) are shown in Table S2

Template	Sequence (5'->3')	Experimental concentration in adjusted reaction circuit (nM)		
		Bistable	Memory	Push-Push
α*to*α	C*C*A*AGACUCAG-CCAA**GACTC**AG	7.5		
β*to*β	A*A*C*AGACUCGA-AACA**GACTC**GA	20		
α*to*iβ	T*T*A*CTCGAAACAGAC-CCAA**GACTC**AG	20		
β*to*iα	T*T*A*CTCAGCCAAGAC-AACA**GACTC**GA	20		
ɣ*to*α	C*C*A*AGACUCAG-GCAT**GACTC**AT		5	
δ*to*β	A*A*C*AGACUCGA-CACT**GACTC**CT		5	10
δ*to*α	C*C*A*AGACUCAG-CACT**GACTC**CT			5
α*to*iδα	T*T*A*CTCAGCACTGAC-CCAA**GACTC**AG			4
β*to*iδβ	A*A*A*CTCGACACTGAC-AACA**GACTC**GA			1

Table S1: Templates and concentrations used in this study. Stars stand for phosphorothioate backbone modifications. Templates are separated in two parts, corresponding to input and output binding sequences, respectively. Nicking enzyme recognition sites are in bold. Uracilated pseudo-sites are in gray.

input / inhibitor	Sequence (5'->3')
α	CT**GAGTC**TTGG
β	TC**GAGTC**TGTT
ɣ	AT**GAGTC**ATGC
δ	AG**GAGTC**AGTG
iα	**GTC**TTGG-CT**GAGT**AA
iβ	**GTC**TGTT-TC**GAGT**AA
iδα	**GTC**AGTG-CT**GAGT**AA
iδβ	**GTC**AGTG-TC**GAGT**TT

Table S2: Input and inhibitors used in this study. Inhibitors are overlapping on both input and output site of their target template. Nicking enzyme recognition sites are in bold, and partial recognition sites (on inhibitors) in gray.

4. Sequence space limitation

With the DNA-toolbox, 11-bases long inputs and 15-bases long inhibitors can be arbitrarily wired in reaction networks following any desired network topology. The shortness of these oligonucleotides is limiting the available sequences: on the 11 bases of an input, 5 are required for the nicking enzyme recognition site (in bold on Table S2), leaving 6 bases to choose among 4 nucleotides. That is 4^6 = 4096 combinations. With a conservative estimate of 2-5 % of them viable (to exclude sequences with secondary structures, G repeats, cross-talks or other issues (e.g. parasitic nicking site)), this leaves about 80-200 sequences. This last number should be compared with the 3 basic sequences needed to build the push-push memory circuit, giving an idea of the maximal circuit complexity that one could construct with the DNA-toolbox (in homogeneous, well mixed conditions).

In order to overcome this limitation, that is, to increase the number of viable input species, one might consider working with longer oligonucleotides (and therefore at higher temperature to maintain the dynamic exchanges). Also, it should be possible to work with another nicking enzyme having a shorter recognition site: this would further increase the available bases for designing inputs with orthogonal sequences.

III. Model

1. Simple Model

Assuming a Michaelis-Menten mechanism for the DNA amplification step of an activation template T = x*to*y,

$$x + T \underset{k_{-1}}{\overset{k_1}{\rightleftarrows}} xT \overset{k_2}{\rightarrow} x + y + T$$

we obtain:

$$\frac{dy}{dt} = \frac{k_2.T.x}{K_x + x};\ K_x = \frac{k_{-1} + k_2}{k_1}$$

where *T* and *x* are the total concentrations of the corresponding species. Note that this is not formaly valid: the second (k_2) reaction involves two complex enzymatic reactions besides mutiple de-hybridization, and thus barely corresponds to the classic Michaelis-Menten assumptions. However, for modelling purposes with minimal mathematical complexity, we can still expect the Michaelis-Menten expression to correctly describe the saturable production of *y* as a function of *x*. From the arguments above, we would also expect $k_2 \ll k_{-1}$, and K_x becomes roughly equal to the dissociation constant of *x* on the template *T*. Moreover, assuming that the inhibiting strand i_{xy} acts as a competitive inhibitor, and noting K_{ixy} the dissociation constant of i_{xy} and k_x the k_2 of activator *x* we obtain:

$$\frac{dy}{dt} = \frac{k_x.T.x}{K_x(1 + \frac{x}{K_x} + \frac{i_{xy}}{K_{ixy}})}$$

For the bistable system as shown in Figure 3*A*, and assuming the same first order degradation rate *D* for all species[2], we can then generalize the previous equation (with obvious notations) to write the complete system as:

$$\begin{aligned}
\frac{d\alpha}{dt} &= \frac{k_\alpha.T_\alpha.\alpha}{K_\alpha(1 + \frac{\alpha}{K_\alpha} + \frac{i_\alpha}{K_{i\alpha}})} - D.\alpha \\
\frac{d\beta}{dt} &= \frac{k_\beta.T_\beta.\beta}{K_\beta(1 + \frac{\beta}{K_\beta} + \frac{i_\beta}{K_{i\beta}})} - D.\beta \\
\frac{di_\alpha}{dt} &= \frac{k_{i\alpha}.T_{i\alpha}.\beta}{K_\beta(1 + \frac{\beta}{K_\beta})} - D.i_\alpha \\
\frac{di_\beta}{dt} &= \frac{k_{i\beta}.T_{i\beta}.\alpha}{K_\alpha(1 + \frac{\alpha}{K_\alpha})} - D.i_\beta
\end{aligned}$$

[2] This is, of course, not realistic, as inhibitors form more stable duplexes than activators, and are "protected" from the exonuclease when in duplex form. Also, note that the exonuclease has different Michaelis constants for inhibitors and activators (SI Appendix, Section III.4). However, in the non-dimensional form of the equations, introducing a different D would come down to scaling $t_{i\alpha}$ and $t_{i\beta}$ and the respective inhibitors concentrations. Therefore it would not change the global dynamic behavior.

We non-dimensionnalize by setting $\tau = t.D$, $\overline{\alpha} = \alpha/K_\alpha$, $\overline{\beta} = \beta/K_\beta$, $\overline{i_\alpha} = i_\alpha/K_\alpha$, $\overline{i_\beta} = i_\beta/K_\beta$, $t_\alpha = k_\alpha.T_\alpha/K_\alpha.D$, $t_\beta = k_\beta.T_\beta/K_\beta.D$, $t_{i\alpha} = k_{i\alpha}.T_{i\alpha}/K_\alpha.D$, $t_{i\beta} = k_{i\beta}.T_{i\beta}/K_\beta.D$, $\lambda_\alpha = K_\alpha/K_{i\alpha}$ and $\lambda_\beta = K_\beta/K_{i\beta}$.

$$\begin{aligned}
\dot{\bar{\alpha}} &= \frac{t_\alpha.\bar{\alpha}}{1+\bar{\alpha}+\lambda_\alpha\bar{i}_\alpha} - \bar{\alpha} \\
\dot{\bar{\beta}} &= \frac{t_\beta.\bar{\beta}}{1+\bar{\beta}+\lambda_\beta\bar{i}_\beta} - \bar{\beta} \\
\dot{\bar{i}}_\alpha &= \frac{t_{i\alpha}.\bar{\beta}}{1+\bar{\beta}} - \bar{i}_\alpha \\
\dot{\bar{i}}_\beta &= \frac{t_{i\beta}.\bar{\alpha}}{1+\bar{\alpha}} - \bar{i}_\beta
\end{aligned}$$

It can be checked that the fixed point $\{\overline{\alpha}, \overline{\beta}\} = \{0, 0\}$ is unstable as soon as one of the autocatalytic templates reach a threshold concentration ($t_\alpha > 1$ *or* $t_\beta > 1$). The two fixed points that can give rise to bistable behavior are then $\{\overline{\alpha}, \overline{\beta}\}$: $\{t_\alpha - 1, 0\}$ and $\{0, t_\beta - 1\}$. They obviously exist only for t_α and t_β superior to unity. Moreover, for the first point, the eigenvalues of the associated Jacobian matrix are $\{-1, -1, (1-t_\alpha)/t_\alpha, -1+t_\alpha.t_\beta/(t_\alpha+\lambda_\beta.t_{i\beta}.(t_\alpha-1))\}$ so this point is stable for $t_\alpha > \lambda_\beta.t_{i\beta}/(1-t_\beta+\lambda_\beta.t_{i\beta})$. Similarly, the second point is stable for $t_\beta > \lambda_\alpha.t_{i\alpha}/(-t_\alpha+1+\lambda_\alpha.t_{i\alpha})$. In the case of a perfectly equilibrated switch $t_\alpha=t_\beta$ and $\lambda_\alpha.t_{i\alpha}=\lambda_\beta.t_{i\beta}$, they may coexist for $\lambda_\alpha.t_{i\alpha} = \lambda_\beta.t_{i\beta} > 1$. Then, the overlapping areas of stability (i.e. the bistable range) will increase with increasing $\lambda_\alpha.t_{i\alpha} = \lambda_\beta.t_{i\beta}$. Finally, a fourth root in the positive quadrant, corresponding to the coexistence of the two dynamic species, can be stable when the two previous inequalities are simultaneously violated (and thus produces a monostable system).

Therefore, the insights brought by this simple model are as follow (see also Fig. 2):

- As soon as their templates reach a threshold concentration, both autocatalytic loops produce a non-trivial steady state in α or β.
- Bistability can occur with asymptotic elimination of one species, but a minimum strength of the inhibitory link is necessary, and the concentrations of the autocatalytic templates must both be within a finite range (below which no species is produced and above which the system is monostable with a single species or two coexistent species).
- The bistable area, which can be interpreted as a quantification of the robustness of the function, increases with increasing inhibiting strength.
- This can be obtained both by increasing the binding constant of the inhibitor or the concentration of the template that produces it. Note however that both cases could result in a breakdown of the assumption used in the model (i.e. inhibitors would not dynamically hybridize anymore or the enzymes would become limiting and the production rate of β would not linearly follow the template concentration).
- The most robust behavior is given by the symmetric (ideal) system, as defined above. However, chemical dissymmetry (for example $k_\alpha \neq k_\beta$) can be compensated by adjusting the concentration of the template responsible for the production of each species.

2. Minimal bistable circuit design: single autoloop

In a system lacking cooperative nonlinearities, bistability can still emerge in the presence of at least one autocatalytic module (51, 55). By using the simple model, we wanted to check if such compact circuit design (one autocatalytic module instead of two) would be deemed feasible in the context of the DNA-toolbox, and if so, how robust would it be compared to the design with two autocatalytic modules.

Experimentally, it should be possible to build a bistable circuit with a single autocatalytic module (Fig. S4-*A*), provided that the concentration of one input species (η) is kept constant (this could be obtained by simply adding phosphorothioate backbone modifications at the 5'-end of η, thus protecting it from degradation by the exonuclease). In the network of Figure S4-*A*, constant input η activates the production of β, which in turn triggers the production of iα, inhibitor of α*to*α. On the other side, α*to*α autocatalytically produces α, which triggers the production of inhibitor iηβ. The latter is targeting template η*to*β, thus inhibiting the production of β.

We constructed a simple model of this circuit (Fig. S4-*B*) and analyzed it the same way as the model of the bistable circuit with two autocatalytic modules (i.e. with the same values of t_{ix}, λ_x and the same ranges of $\{t_\alpha, t_\beta\}$). The phase diagrams of this bistable circuit in the plane $\{t_\alpha, t_\beta\}$ (Fig. S4-*C* and *D*) suggest that in the context of the DNA-toolbox, and using similar design rules, this single-autocatalytic module design is less robust than the design containing two autocatalytic modules (analyzed in Figure 2 of the main text). Moreover, it does not deliver a symmetric output to signal its current state.

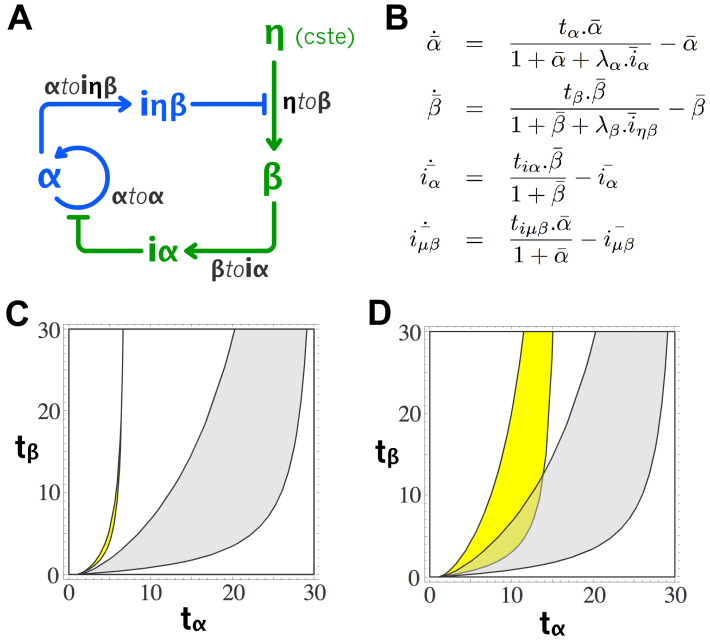

Figure S4: (A) Single-autocatalytic module circuit encoding bistability. (B) Non-dimensionalized equations of the simplified model. t_x are the scaled concentrations of template producing x and λ_x the ratio of activator over inhibitor binding constant. Periods indicate multiplications. (C) Phase diagram of the bistable circuit in the plane $\{t_\alpha, t_\beta\}$, with $\{t_{i\alpha}, t_{i\eta\beta}\}$ = {0.3, 0.3} and $\bar{\eta}$ = 1. Yellow: bistable domain for $\{\lambda_\alpha, \lambda_\beta\}$ = {20, 20}. Gray: bistable domain for $\{\lambda_\alpha, \lambda_\beta\}$ = {100, 100}. (D) Idem with yellow: bistable domain for $\{\lambda_\alpha, \lambda_\beta\}$ = {50, 100}; and gray: bistable domain for $\{\lambda_\alpha, \lambda_\beta\}$ = {100, 100}.

3. Simple robustness

Using the simple nondimensionalized model, we assessed the response of the bistable switch to perturbation in its input concentrations. In this simplified, "instantaneous" model (i.e. that strictly relies on the instantaneous concentrations of dynamic species and does not incorporate hybridization / dehybridization dynamics), the bistable flips between states as soon as the injected OFF state input exceeds the ON state input (Fig. S5).

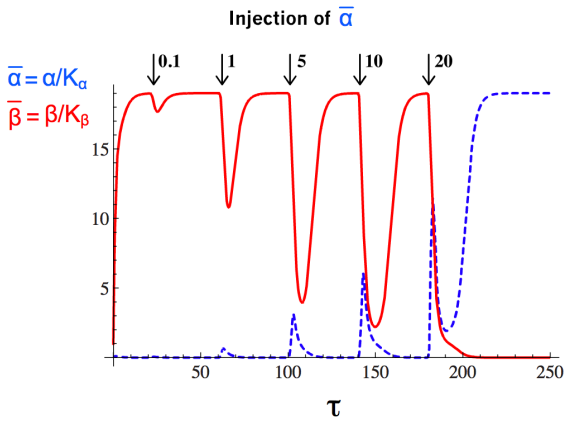

Figure S5: Assessing the response of the bistable switch: successive Gaussian spikes of increasing amount of $\overline{\alpha}$ are added to the system in the B state. $\overline{\beta}$ (red line) responds by a decrease as $\overline{\alpha}$ (blue dashed line) is injected. Eventually, injected $\overline{\alpha}$ transiently exceeds the amount of $\overline{\beta}$ at the steady state: the bistable flips from B to A. The parameters are $t_\alpha = t_\beta = 20$, $t_{i\alpha} = t_{i\beta} = 0.3$, $\lambda_\alpha = \lambda_\beta = 100$.

4. Detailed Model construction

Whereas the simple model gives a good insight about the validity of a given circuit design and its steady states, it fails to predict realistically the experimental circuit dynamics. Thus we built a more detailed mathematical model that takes in account all the hybridization and enzymatic reactions that happen in a toolbox-based DNA reaction circuit (as an example, see the detailed set of reactions for a circuit constituted of one autocatalytic module on Figure S6), with the following assumptions:

- Association rate of k_a = 0.06 $nM^{-1}.min^{-1}$ was taken, as proposed by Zhang and Winfree (64) for short oligonucleotides.

- Also, inhibitors take advantage of a 7 bases (if hybridizing to template-output duplex) or 6 bases (if hybridizing to template-input duplex) toehold: at 25 °C, this should give them a full hybridization speed (64). Our working temperature is however higher, and should decrease the efficiency of these toeholds, but, since we are about 1 or 2 °C higher than the T_m of inputs, and inhibitors bind about 100x tighter than inputs, we still make the assumption that inhibitors can hybridize to templates occupied by either input or output with hybridization rate k_a, (i.e. as if hybridizing to an unoccupied template). Then, the rate of the reverse reactions ("input (or output) displacing inhibitor") can be calculated from the equilibrium constant of the reaction, i.e. the difference in affinity between activators and inhibitors, which we approximated for every sequence at toe = 10^{-2}.

- *Bst* DNA polymerase and ttRecJ are processive enzymes, so we assume that there is no accumulation of partially polymerized or partially degraded inputs or inhibitors.

- Enzymes rates and Michaelis constants were kept to the same value for all DNA substrates. When fitting experimental curves, we adjusted (by hand) the specific dissociation rate of each species to compensate for the substrate dependency of enzymatic rates and affinity.

From a first set of measured or predicted[3] parameters, we used the experimental curves of Figure 6*E* (main text) to optimize the enzymatic and thermodynamic parameters (Table S3). This set of adjusted parameters was then used for all the simulations presented in this work, including the push-push memory circuit. In this last case, for the two additional inhibitors (iδα and iδβ), we directly used dissociation constants calculated with DINAMelt[3].

In the context of the DNA-toolbox, it is possible to obtain a very good computational estimate[3] of the dissociation constants of the different species: inhibitors iα and iβ were chosen for their predicted dissociation constants (4.8 nM^{-1} for iα and 1.1 nM^{-1} for iβ) that were in the desired range (i.e. about two order of magnitude higher than α and β). These parameters can also be easily

[3] Using DINAMelt (http://mfold.rna.albany.edu/?q=DINAMelt)

measured with a DNA melting experiment, which gave the values used in the detailed model (4.8 nM^{-1} for iα and 1.4 nM^{-1} iβ). Experimental and predicted values are very close, which is a great advantage compared to the system previously reported by Montagne *et al.*, where the presence of trehalose (used to stabilize the mesophilic exonuclease $RecJ_f$) and EvaGreen (intercalating dye) impacted on the melting behavior of DNA duplexes and were hindering the direct estimation of the thermodynamic values using standard algorithms (23).

Enzymatic parameters were measured using the assays previously described in Montagne *et al.* (23). For ttRecJ, we found similar enzymatic rates for α, β, iα and iβ (300±8 nM/min) and roughly similar Michaelis constant for inhibitors iα and iβ (150±10 nM). However, we found Michaelis constant for input α and β to be higher (440±100 nM), suggesting a higher affinity of ttRecJ for longer substrates (inhibitors). This was also the case for $RecJ_f$ used in Montagne *et al*. (23). We thus assigned two different parameters for inputs and inhibitors. For Nt.BstNBI, we found Michaelis constants of 30±10 nM for α and β. We however kept one single value for all input species, which would be compensated by adjusting each input dissociation rate during the fitting process.

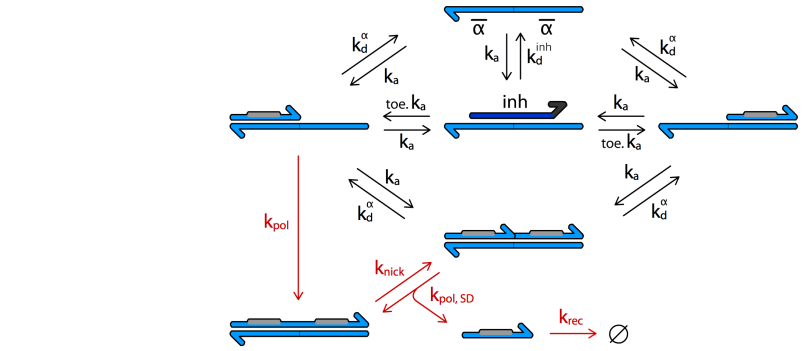

$$A'(t) = k_d^\alpha . (\mathrm{A}\alpha(t) + \alpha\mathrm{A}(t)) + k_d^{inh} . \mathrm{Ainh}(t) - k_a . A(t) . (2\,\alpha(t) + \mathrm{inh}(t))$$

$$\alpha\mathrm{A}'(t) = k_a . \alpha(t) . (A(t) - \alpha\mathrm{A}(t)) + \mathrm{toe} . k_a . \alpha(t) . \mathrm{Ainh}(t) + k_d^\alpha . \alpha\mathrm{A}\alpha(t) - k_a . \mathrm{inh}(t) . \alpha\mathrm{A}(t) - k_d^\alpha . \alpha\mathrm{A}(t) - \frac{k_{pol}\,\alpha\mathrm{A}(t)}{K_m\left(\frac{\alpha\mathrm{A}\alpha(t)}{K_{m,SD}} + \frac{\alpha\mathrm{A}(t)}{K_m} + 1\right)}$$

$$\mathrm{A}\alpha'(t) = k_a . \alpha(t) . (A(t) - \mathrm{A}\alpha(t)) + \mathrm{toe} . k_a . \alpha(t) . \mathrm{Ainh}(t) + k_d^\alpha . \alpha\mathrm{A}\alpha(t) - k_a . \mathrm{inh}(t) . \mathrm{A}\alpha(t) - k_d^\alpha . \mathrm{A}\alpha(t)$$

$$\mathrm{A}\alpha\alpha'(t) = \frac{k_{pol} . \alpha\mathrm{A}(t)}{K_m\left(\frac{\alpha\mathrm{A}(t)}{K_m} + \frac{\alpha\mathrm{A}\alpha(t)}{K_{m,SD}} + 1\right)} + \frac{k_{pol,SD} . \alpha\mathrm{A}\alpha(t)}{K_{m,SD}\left(\frac{\alpha\mathrm{A}\alpha(t)}{K_{m,SD}} + \frac{\alpha\mathrm{A}(t)}{K_m} + 1\right)} - \frac{k_{nick} . \mathrm{A}\alpha\alpha(t)}{K_{mn}\left(\frac{\mathrm{A}\alpha\alpha(t)}{K_{mn}} + 1\right)}$$

$$\alpha\mathrm{A}\alpha'(t) = k_a . \alpha(t) . (\mathrm{A}\alpha(t) + \alpha\mathrm{A}(t)) - 2\,k_d^\alpha . \alpha\mathrm{A}\alpha(t) + \frac{k_{nick} . \mathrm{A}\alpha\alpha(t)}{K_{mn}\left(\frac{\mathrm{A}\alpha\alpha(t)}{K_{mn}} + 1\right)} - \frac{k_{pol,SD} . \alpha\mathrm{A}\alpha(t)}{K_{m,SD}\left(\frac{\alpha\mathrm{A}\alpha(t)}{K_{m,SD}} + \frac{\alpha\mathrm{A}(t)}{K_m} + 1\right)}$$

$$\mathrm{Ainh}'(t) = k_a . \mathrm{inh}(t) . (A(t) + \mathrm{A}\alpha(t) + \alpha\mathrm{A}(t)) - 2\,\mathrm{toe} . k_a . \alpha(t) . \mathrm{Ainh}(t) - k_d^{inh} . \mathrm{Ainh}(t)$$

$$\alpha'(t) = k_d^\alpha . (\mathrm{A}\alpha(t) + \alpha\mathrm{A}(t) + 2\,\alpha\mathrm{A}\alpha(t)) + k_a . \mathrm{inh}(t) . (\mathrm{A}\alpha(t) + \alpha\mathrm{A}(t)) - k_a . \alpha(t) . (2\,A(t) + \mathrm{A}\alpha(t) + \alpha\mathrm{A}(t) + 2\,\mathrm{toe} . \mathrm{Ainh}(t)) + \frac{k_{pol,SD} . \alpha\mathrm{A}\alpha(t)}{K_{m,SD}\left(\frac{\alpha\mathrm{A}\alpha(t)}{K_{m,SD}} + \frac{\alpha\mathrm{A}(t)}{K_m} + 1\right)} - \frac{k_{rec} . \alpha(t)}{K_{m,input}\left(\frac{\alpha(t)}{K_{m,input}} + \frac{\mathrm{inh}(t)}{K_{m,inh}} + 1\right)}$$

Figure S6: Schematic of the full set of reactions relative to a reaction circuit where input α only interacts with template αtoα, and the corresponding set of ordinary differential equations. αtoα is noted A for simplicity of notation. Red arrows indicate enzymatic reactions. Periods indicate multiplications. Dissociation rates (in min^{-1}) were calculated as $k_d = k_a/K_d$.

			Starting values	Fitted values	Drift from starting values
Association rate ($nM^{-1}.min^{-1}$)		k_a	0.06	0.06	0
Dissociation constants (nM^{-1})		K_d^{α}	**0.014**	0.013	-8%
		K_d^{β}	**0.006**	0.0045	-25%
		$K_d^{i\alpha}$	**4.8**	5.3	+10%
		$K_d^{i\beta}$	**1.4**	1.3	-8%
		K_d^{γ}	0.007	0.016	+128%
		K_d^{δ}	0.02	0.038	+90%
		$K_d^{i\delta_{\alpha}}$	4.8	4.8	0
		$K_d^{i\delta_{\beta}}$	3.5	3.5	0
Enzymatic maximum rates ($nM.min^{-1}$)	*Bst* DNA polymerase	k_{pol}	**1200***	2100	*
		$k_{pol,SD}$	**40***	420	*
	Nt.BstNBI	k_{nick}	**58 ~ 720**	80	
	$ttRecJ_f$	k_{rec}	**300**	300	0
Michaelis constants (nM)	*Bst* DNA polymerase	K_m	**44***	80	*
		$K_{m,SD}$	**3.5***	5.5	*
	Nt.BstNBI	K_{mn}	**30**	30	0
	$ttRecJ_f$	$K_{m,input}$	**440**	440	0
		$K_{m,inh}$	**150**	150	0

*Table S3: Set of parameters of the detailed model. Values in bold were experimentally measured. Dissociation constants were otherwise predicted using Dinamelt. *Enzymatic parameters for Bst DNA polymerase were measured in different conditions (at 38.5 °C instead of 42 °C and in a different buffer (23)), making irrelevant the calculation of a drift from the starting values. We noticed one order of magnitude fluctuations in the batch-to-batch activity of the commercial nicking enzyme Nt.BstNBI sold by New England Biolabs. Consequently, we needed to adjust the concentration of this enzyme in the interval from 32 to 400 units/mL, in order to get consistent experimental results, using the assay of Figure S3 for each new batch. After this experimental adjustment of the concentration of nicking enzyme, we kept a single value of k_{nick} for the simulations.*

5. Perturbation of the bistable and switching threshold

As shown in Figure S5, the simple model fails to describe the actual resilience of the bistable to perturbation in concentration of its inputs (α and β). We thus used the detailed model of the bistable, let it settle on its steady state for 100 minutes, and then added pulses of α or β (as Gaussian spikes). In Figure S7, we plot the state (A or B) of the bistable 500 minutes after the injection, as a function of the normalized concentration of injected input, for example α/β_{ss} (ratio of injected α on concentration of β at the steady state) or β/α_{ss} (ratio of injected β on concentration of α at the steady state). Both sides appear to behave relatively symmetrically, and require an injection of opposite input of more than 20-fold the concentration of input at the steady-state, in order to flip between states.

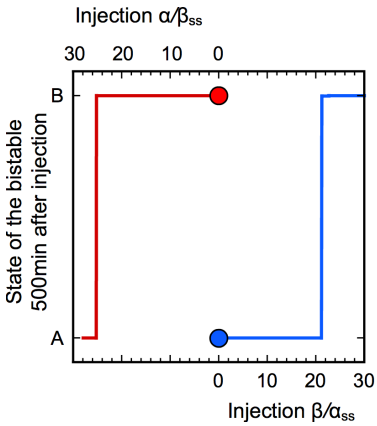

Figure S7: Numerical simulation of the switching of the bistable with the detailed model. The system, initially in state A (blue dot) or B (red dot) is perturbed by a Gaussian spike of input of the opposite species, from 0 to 30-fold the current steady concentration. The plot gives the state observed 500 minutes after the injection.

6. Activation module

An activation module is a template that amplifies a short spike of its input into a long-lasting pulse of its output. As an example, activation module δ*to*β is activated by δ, but also acts as a "refuge" for δ: in hybridized (and elongated) state, δ is protected from ttRecJ that specifically targets single-stranded substrates. δ is thus able to stay in solution for longer than without "refuge" templates, and thus activate the production of a long-lasting pulse of β. Figure S8 shows the predicted time plot of α and β concentrations produced by 5 nM of the corresponding activation module, compared to a direct injection of α and β.

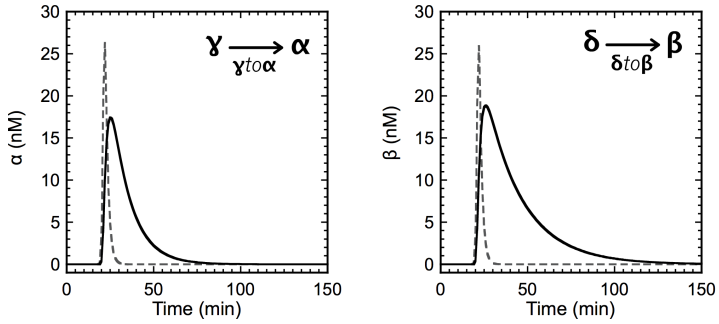

Figure S8: Predicted time plots of the concentration of α (left) and β (right) produced by the activation module ɣtoα or *δtoβ (5 nM) upon injection of 30 nM of the corresponding input ɣ or δ. These curves (plain lines) are compared to direct spike of 30 nM of α or β (dashed lines). These predictions were generated with the detailed model.*

7. Push-push strategy

In the push-push memory circuit, the current state of the bistable core is fed back to the two activation modules. This allows the system to decide which internal specie (α or β) to produce upon reading of the single external input δ, depending on its current state. We checked the validity of this strategy with the detailed mathematical model. In the absence of autocatalytic modules α*to*α and β*to*β (Fig. S9-*A*), we impose a fixed concentration (40 nM) of non-degradable internal input α or β, and set a spike of 30 nM of external input δ. Figure S9-*B* shows that the system responds with the production of a large pulse of the species that is initially absent (i.e. β if the system is in A state, and conversely). Still, the model predicts that the charge level of β*to*iα (for β imposed) and α*to*iβ (for α imposed) is transiently slightly exceeding 1, which indicates a small leak production of the current internal species. Note that no switching is expected here since the state is externally imposed at all times (and no autocatalytic module is present).

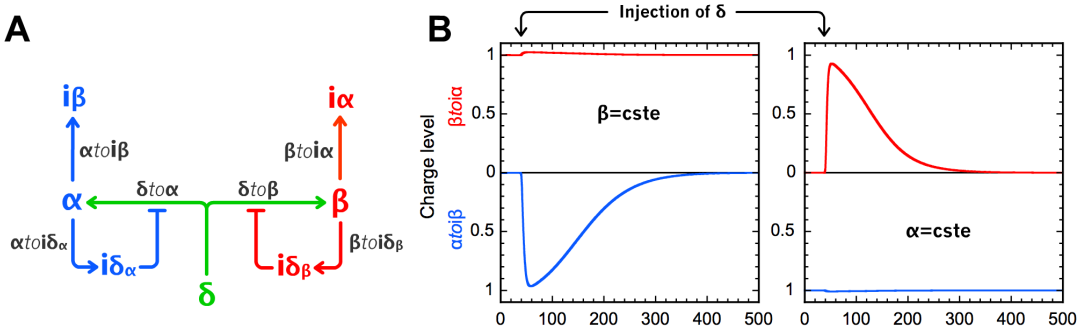

Figure S9: Structure and function of the injection layer for the push-push memory system. (A) Inhibition modules αtoiδα and βtoiδβ produce respectively iδα and iδβ, depending on the presence of either α or β. Inhibitors iδα and iδβ inhibit the activation modules δtoα and δtoβ. In the resulting circuit, in the presence of α, δtoα is inhibited, and injection of the external input δ will only activate δtoβ, hence produce β. Conversely, in presence of β, only δtoα will be sensible to external input δ. (B) Theoretical time traces of the charge level of the templates βtoiα and *αtoiβ either when the constant presence of α is imposed and a short pulse of δ is applied (left), or when the constant presence of β is imposed and the same short pulse of δ is applied (right).*

IV. Reamplification

Here, we used a previously reported method (23) to experimentally measure the concentrations of α and β when the bistable switch is asymptotically converging toward one or the other of its two dynamic stable states.

The system was initiated with {α, β} = {10 nM, 0.1 nM} or {0.1 nM, 10 nM}, and allowed 150 minutes to reach one of its steady states, respectively A or B (as judged by the fluorescence signals). We then withdrew aliquots from the solutions and immediately quenched them by 10x dilution in 95 °C mQ water followed by a 5 minutes incubation at the same temperature. Dilution of these samples were then amplified by isothermal amplification at 50 °C in presence of template α*to*α (20 nM) or β*to*β (30 nM) with *Bst* DNA polymerase (8 units/ml) and Nt.BstNBI nicking endonuclease (100 units/ml). The reaction was performed in a thermocycler set at a constant temperature (50 °C) and monitored with 1x EvaGreen intercalating dye as described. Using the built-in software, concentrations of α and β were determined from the shape of the amplification curves by comparison with calibration curves built from UV-calibrated concentrations of pure α or β. Results are displayed in Table S4.

	α		β	
Bistable state	A	B	A	B
Sample dilution	1000	100	100	1000
Measured Concentration (pM)	55	0.82	0.68	40
Concentration in aliquots (nM)	55±2	0.082±0.008	0.068±0.004	40±7

Table S4: Measured concentrations of α and β at the steady state of the bistable in state A and B.

V. Push-push memory circuit

In the assembly of the push-push memory circuit, we kept the templates of the bistable core at the same concentrations as for the memory circuit and the bistable circuit, and adjusted the concentration of the 4 templates that encode the push-push function. The detailed model suggested that the full circuit would work with concentrations of activation modules δ*to*α and δ*to*β at 5 nM and inhibition modules α*to*iδα and β*to*iδβ at 4 nM. In these conditions, upon addition of 30 nM of *δ,* the experimental push-push circuit successfully switched from B to A, but failed to switch from A to B (Fig. S10). This result pointed out that a stronger amplification of input β was required to push the circuit (initially in state A) to the basin of attraction of state B. We consequently adjusted the concentrations of δ*to*β (to 10 nM) and β*to*iδβ to obtain a working point where the push-push memory circuit could switch in both directions. Table S5 displays the experimental results of the fine-tuning of the concentration of β*to*iδβ, showing that the strength of the negative feedback (performed by β*to*iδβ) must be carefully adjusted in order to reach a reversible working point. Experimental trajectories of the push-push memory circuit (Figure 7*C* of the main text) are shown as time plots on Figure S11.

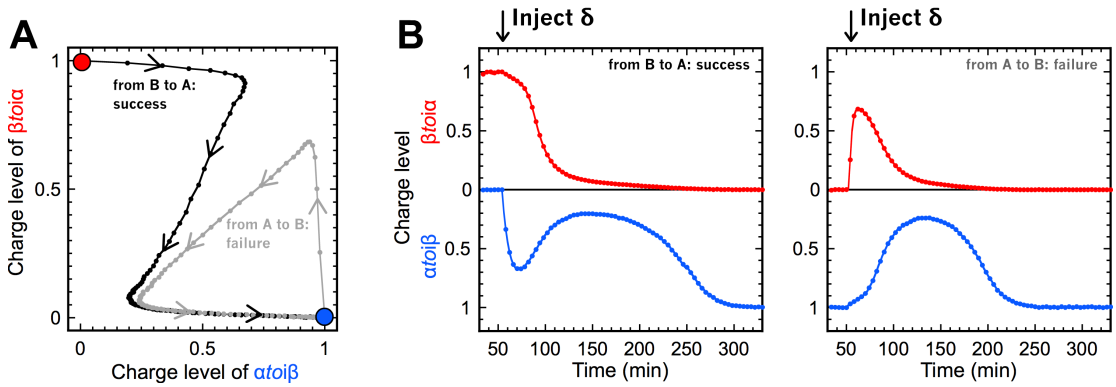

Figure S10: Experimental trajectories (A) and time plots (B) of the push-push memory circuit with δtoα = δtoβ = 5 nM and αtoiδ$_α$ = βtoiδβ = 4 nM. Upon addition of 30nM of *δ, the circuit switched from B to A, but failed to switch from A to B.*

	Switching from	
[β*to*iδβ] (nM)	A->B	B->A
0.6	✓	
0.8	✓	
1	✓	✓
1.2		✓

Table S5: Experimental result of the push-push memory circuit (with δtoβ = 10 nM, δtoα = 5 nM and αtoiδα = 4 nM) flipping between states for different concentrations of inhibition module βtoiδ$_β$.

The discrepancy between the predicted concentrations (δ*to*β = 5 nM, β*to*iδβ = 4 nM) and the ones that gave good experimental results (δ*to*β = 10 nM, β*to*iδβ = 1 nM) can be explained by the method we used to adjust the model parameters. As detailed in SI Appendix, Section III.4, we took the same enzymes parameters for all substrates, then compensated the substrate-dependent enzymatic rates and

Michaelis constants by adjusting the specific dissociation rate of each input and inhibitor.

This method worked well in the case of the two-input memory circuit, where each input activates only one activation module. In the push-push memory circuit, however, δ activates both δ*to*α and δ*to*β, forming two substrates for which polymerase and nickase are likely to display different rates and affinities. These won't be possible to equilibrate as we adjust a single parameter for δ. In reality, δ might also have two different binding constants for δ*to*α and δ*to*β: ideally, one would have to independently measure the hybridization / dissociation kinetics of all duplexes, and enzymatic rates and Michaelis constants for all substrates. In the present study, we showed that we could obtain a relatively good agreement between the detailed model and the experiments without going into such details.

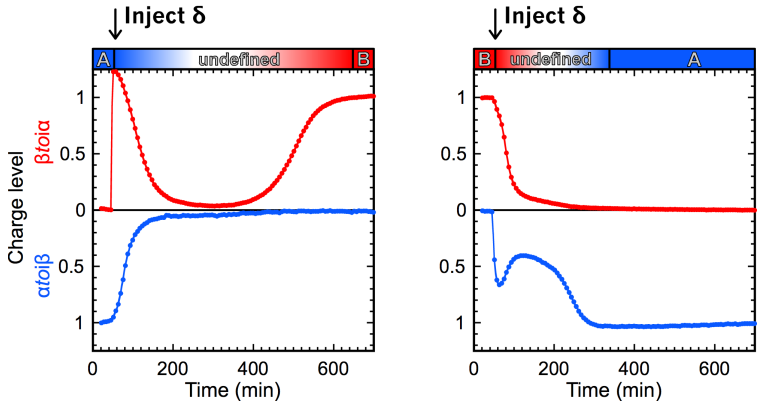

Figure S11: Experimental time plots (same data as Figure 7 (main text)) of the push-push memory circuit with δtoα = 5 nM, δtoβ = 10 nM, αtoiδ$_\alpha$ = 4 nM, and βtoiδβ = 1 nM. Upon addition of 30nM of *δ, the circuit switched from A to B (left), and from B to A (right).*

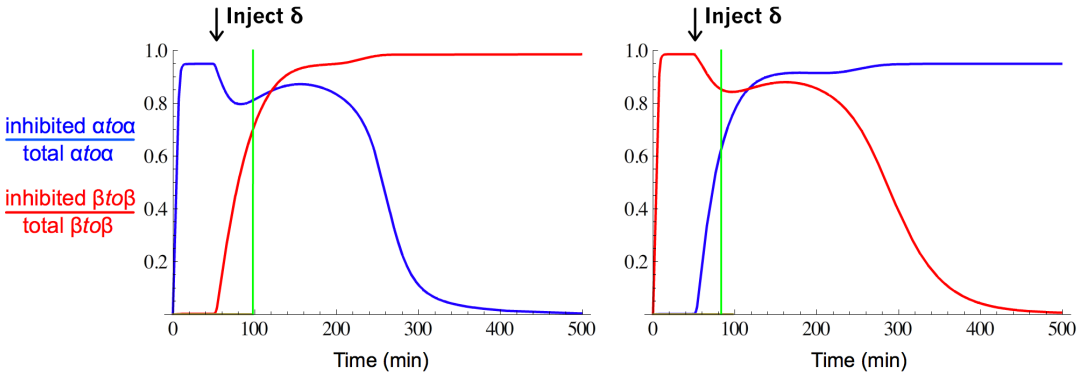

Figure S12: Predicted time plots of the proportion of inhibited αtoα and βtoβ during a switching of the push-push from B to A (left) and A to B (right). The green line shows where the trajectories apparently cross on Figure 7 (main text): one observes that they in fact correspond to two different proportions of inhibited αtoα and βtoβ.

VI. Long-term experiments

One Figure 6 of the main text, we showed that the two-input memory circuit could be switched from one state to the other, then back to the initial state. However, further switching was not successful. Similarly, re-activating the push-push system after a first switch did not result in a complete switching. These observations should probably be attributed to the very long time that is necessary to perform such experiments: in the case of the two-input memory circuit, each switching event takes about 200 minutes (Fig. 6) and in the case of the push-push network, up to 600 minutes (Fig. S11-left). Over this extended time, dNTPs will unavoidably deplete, enzymes loose activity and template strands decrease in concentration. Our best hypothesis to explain these experimental observations is that one of these changes, or possibly a combination of some of them, will ruin the delicate balancing of the various reactions, which is necessary for the correct functioning of the circuit[4]: one may imagine that a decreased, say, nicking activity may favor one side of the switch over the other, and this would drive the system away from its bistable area. Moreover, because the bistable core is continuously active over the course of the reactions (continuously producing –and degrading– new oligonucleotides), it is possible that side reactions, even with low probability or very slow rates, may ultimately produce deleterious effect on the circuit.

This hypothesis is supported by experiments showing that the activity of various subparts of the networks do change over time, and not necessarily in a proportional or predictable manner. Two such simple experiments are presented on Figure S13. On the experiment of Figure S13-*A*, autocatalytic module α*to*α is activated once upon administration of a small quantity of dNTPs, and is then left in the presence of the three enzymes, but no dNTPs, for a thousand minutes. When activated again with the same amount of dNTPs, α*to*α does not amplify as sharply and takes more time to consume all the dNTPs. The experiment of Figure S13-*B* shows two successive inhibitions of α*to*α: here also, α*to*α is more strongly inhibited during the second inhibition. On the one hand, this suggests a loss of activity of α*to*α, but on the other hand, this shows that β*to*iα is still handling well its function. These two experiments suggest that it may indeed be some variation in the relative "strength" of the subparts that leads to the loss of function of the global system.

[4] With this hypothesis, the fact that the *Oligator* of Montagne *et al.* could still oscillate after 4000 minutes could be attributed to a higher robustness of the network design, which does not rest upon the delicate balance of two symmetrical nodes. It is also probable that the complete switching between two autocatalytic modules that happens in the bistable circuit (i.e. extinction of one and establishment of a steady state of the other) puts more strain on the system than a complete cycle of the Oligator (where the autocatalytic module never gets to 0 nor to its steady state concentration, but oscillate around a value somewhere in between). The fact that the operation of the two-input memory circuit requires repetitive additions of small volumes of input (hence changes in concentration of the constituents of the system) may also have an impact on the long-term functioning of the system.

Below, we tentatively discuss one of the many mechanisms that may lead to such evolution over time and possibly hinder the long-term performance of the circuit.

One issue may lay in the slow degradation of the templates by the exonuclease (Fig. S2). In Section V, we have seen that the push-push memory circuit was very sensible to a variation in template concentration: the circuit worked for 1 nM of β*to*iδβ, but its ability to switch in both directions was lost when this value was increased or decreased by 20%. As a circuit is running, the exonuclease may slowly degrade all the templates, potentially disrupting the ratios of templates concentrations in the circuit; it turns out that we have not found a perfect protection against ttRecJ. Besides, the actual behavior of ttRecJ with respect to phosphorothioate (PT) linkages (used to protect the 5' end of all templates) is not known.

PT linkages are inherently chiral: Yang *et al.* (65) reported that Exonuclease III stops on R isomers, but digests S ones. If ttRecJ was to behave the same, we would have, roughly, 50% of intact templates, 25% of templates with 1 base missing, 12,5% of templates with 2 bases missing, and 12,5% of templates entirely digested. In the case where PT linkages would just slow down ttRecJ, all templates would be degraded little by little throughout the reaction. Given the results of Figure S2, we might be facing both behaviors at the same time: degradation curves for 2 PT and 3 PT display an initial quick decrease, then a slower linear slope.

In any case, templates are likely to loose activity because of (*i*) decrease of their concentration, (*ii*) loss of one or two bases in 5', which would results in the production of truncated output (with one or two bases missing in 3'), less stable on their target template (i.e. weaker activators). Then, an explanation for the results shown on Figure S13-*B* (i.e. inhibition module β*to*iα still properly handling its function) would be that inhibition modules spend most of their time in duplex with the inhibitor that they produce (iα has a predicted T_m of 51.3 °C on β*to*iα): in this duplex form, they are protected from the single-stranded specific exonuclease and consequently degrade more slowly.

Note however that the mechanism discussed above would not explain the difference in durability of two similar templates like α*to*α and β*to*β, but more a departure from the general balance of the system.

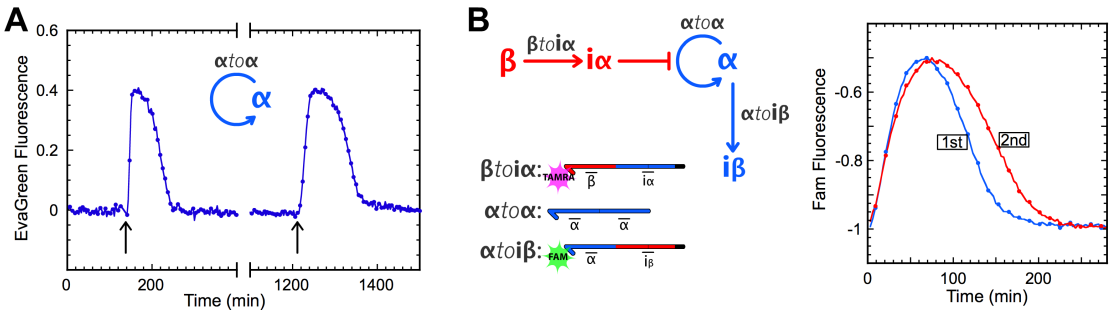

Figure S13: Checking the viability of the circuit over time. (A) Autocatalytic module αtoα (20 nM) is given dNTPs (20 μM) and input α (1 nM) at the times marked by an arrow: first at t = 140min, then at t = 1220 min. After having consumed all dNTPs, it stops producing α: fluorescence level gets back to the baseline level. Reaction is monitored with EvaGreen intercalating dye that reports on the total amount of double-stranded DNA in solution. (B) Autocatalytic module αtoα (5 nM) is inhibited by iα produced by βtoiα (20nM) upon injection of β (80 nM). Reaction is monitored with the FAM label of αtoiβ (20 nM): fluorescence increases as αtoα is inhibited. Following a first inhibition (blue curve) a second is triggered 500 minutes later (red curve).

VII. Supplementary References

60. Qian J et al. (2012) Sequence dependence of isothermal DNA amplification via EXPAR. *Nucleic Acids Res* 40:e87.

61. Mazurek M, Sowers L (1996) The paradoxical influence of thymine analogues on restriction endonuclease cleavage of oligodeoxynucleotides. *Biochemistry* 35:11522–11528.

62. Pang J, Modlin J, Yolken R (1992) Use of Modified Nucleotides and Uracil-DNA Glycosylase (UNG) for the Control of Contamination in the PCR-Based Amplification of RNA. *Mol Cell Probe* 6:251–256.

63. Greagg MA et al. (1999) A read-ahead function in archaeal DNA polymerases detects promutagenic template-strand uracil. *Proc Natl Acad Sci USA* 96:9045–9050.

64. Zhang DY, Winfree E (2009) Control of DNA strand displacement kinetics using toehold exchange. *J Am Chem Soc* 131:17303–17314.

65. Yang Z, Sismour AM, Benner SA (2007) Nucleoside alpha-thiotriphosphates, polymerases and the exonuclease III analysis of oligonucleotides containing phosphorothioate linkages. *Nucleic Acids Res* 35:3118–3127.